UCSF

Title

Slit pores preferred over cylindrical pores for high selectivity in biomolecular filtration

Permalink

https://escholarship.org/uc/item/027737h5

Authors

Feinberg, Benjamin J
Hsiao, Jeff C
Park, Jaehyun
et al.

Publication Date

2018-05-01

DOI

10.1016/j.jcis.2017.12.056

Peer reviewed

Slit pores preferred over cylindrical pores for high selectivity in biomolecular filtration

Benjamin J. Feinberg[1], **Jeff C. Hsiao**[1], **Jaehyun Park**[1], **Andrew L. Zydney**[2], **William H. Fissell**[3], and **Shuvo Roy**[1]

[1]Department of Bioengineering and Therapeutic Sciences, University of California, San Francisco, California, USA

[2]Department of Chemical Engineering, The Pennsylvania State University, University Park, PA

[3]Department of Medicine and Division of Nephrology and Hypertension, Vanderbilt University, Nashville, TN

Abstract

Microelectromechanical systems (MEMS) have enabled the fabrication of silicon nanopore membranes (SNM) with uniform non-overlapping "slit shaped" pores. The application of SNM has been suggested for high selectivity of biomolecules in a variety of medical filtration applications. The aim of this study was to rigorously quantify the differences in sieving between slit pore SNM and more commonly modeled cylindrical pore membranes, including effects of the extended Derjaguin, Landau, Verwey, and Overbeek (XDLVO) interactions. Applying equations derived for SNM in previous work, we compare the partition coefficient of slit and cylindrical pore membranes while accounting for both steric and XDLVO interactions. Simple, steric approximations demonstrate that slit pore membranes exhibit significantly lower partition coefficients than cylindrical pore models. Incorporating XDLVO interactions results in an even more marked difference between slit pore and cylindrical pore membranes. These partition coefficients were used to evaluate changes in beta-2-microglobulin (B2M) selectivity. The data demonstrate that XDLVO interactions increase the selectivity advantage that slit pores possess over cylindrical pores, particularly for larger values of the acid-base decay constant. Finally, the bovine serum albumin (BSA) to B2M selectivity ratio was investigated. The selectivity ratio appears larger in slit pores than cylindrical pores for all cases, indicating that slit pores are particularly well suited for hemofiltration applications. The results of this study have significant implications for the application of SNM in membrane processes where highly selective separations of biomolecules is desirable.

Graphical abstract

Correspondence to: Shuvo Roy.
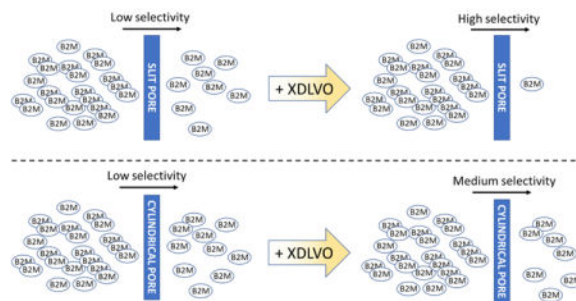
Keywords

Membrane transport; XDLVO; MEMS; silicon nanopore membran

---

1. Introduction

Recently, our laboratory has developed novel silicon nanopore membranes (SNM) using microelectromechanical systems (MEMS) technology. These membranes possess a nearly uniform pore size and zero pore overlap. The development of SNM has enabled new applications in biomedical engineering, including an artificial implantable kidney, bioartificial pancreas, and extracorporeal membrane oxygenator [1][2][3]. Earlier work from our group compared the unique slit pore structure of SNM with the traditional cylindrical pore membranes [4]. This analysis showed that slit pores offer higher selectivity than cylindrical pores at a given scaled membrane permeability, but this work only considered the effects of solute size (i.e. steric considerations). We recently published a comprehensive transport model for the unique slit pore structure of SNM that includes, for the first time, a consideration of intermolecular interactions between the membrane and solute in the unique slit pore geometry. These interactions, which include van der Waals (LW), acid-base (AB), and electrostatic (EL) forces, can have a significant impact on the transport of solutes through the membrane [5]. Collectively, these forces comprise the extended Derjaguin, Landau, Verwey, and Overbeek (XDLVO) theory.

The development of the XDLVO slit pore model now allows for comprehensive comparison of solute transport through membranes composed of an array of classic cylindrical pores and SNM slit pores. While steric ("size based") models provide for facile comparison between slit pores and cylindrical pores, they do not account for the interaction between solutes and the membrane pore surface. The purpose of this study is to compare the selectivity of slit pore and cylindrical pore membranes accounting for a wide range of solute-membrane interactions.

2. Model Formulation

2.1. Membrane transport equations

The general equations for solvent and mass transport through membranes are discussed in detail in the existing literature [6]. Briefly, water transport, J_w, across the membrane can be written as

$$J_w = L_p(\Delta P - \sigma \Delta \pi) \quad \text{Eq 1}$$

where L_p is the hydraulic permeability of the membrane, P is the hydraulic pressure difference across the membrane, π is the osmotic pressure difference, and σ is the osmotic reflection coefficient. The hydraulic permeability, which is calculated by solving the Navier-Stokes equations for fluid flow, is defined as

$$L_{p,\text{slit}} = \frac{\varepsilon h^2}{3\mu\delta_m} \quad \text{Eq 2}$$

$$L_{p,\text{cyl}} = \frac{\varepsilon r_p^2}{8\mu\delta_m} \quad \text{Eq 3}$$

for slit pores and cylindrical pores, respectively. In Eq 2 and Eq 3, μ is the fluid viscosity, δ_m is the membrane thickness, ε is the membrane porosity, r_p is the cylindrical pore radius, and h is the slit pore half width. To calculate the 'scaled' permeability, the individual permeability value is multiplied by the factor $\mu\delta_m/\varepsilon$. Note that Eq 2 and Eq 3 neglect the effects of counter-electroosmosis on fluid flow [7].

Solving the differential equations for convective and diffusive transport across the membranes yields the actual sieving coefficient, S_a,

$$S_a = \frac{c_f}{c_{b,m}} = \frac{S_\infty \exp(\text{Pe})}{S_\infty + \exp(\text{Pe}) - 1} \quad \text{Eq 4}$$

where c_f is the solute concentration in the filtrate, $c_{b,m}$ is the solute concentration in the feed solution at the membrane surface, S_∞ is the asymptotic sieving coefficient corresponding to convective transport alone, and Pe is the Peclet number, i.e. the ratio of convective to diffusive transport in the membrane [8]. The Peclet number itself is calculated through Pe = $J_w\delta_m S_\infty/\varepsilon\phi K_d D_\infty$, where ϕ is the solute-membrane partition coefficient, K_d is the diffusive hindrance factor, and D_∞ is the bulk diffusion coefficient of the solute [8]. The asymptotic sieving coefficient $S_\infty = \phi K_c$, is the sieving coefficient at very high Peclet number and is equal to the product of ϕ and the convective hindrance factor, K_c. The selectivity of a membrane for a given solute is simply the inverse of the sieving coefficient.

Two simplifications have been applied in order to deconvolute the comparison of slit and cylindrical pores. First, the selectivity considered in the rest of this paper is measured as the inverse of the asymptotic sieving coefficient (i.e. $1/S_a = 1/S_\infty$), which strictly applies only when convection dominates diffusion. This allows for easy comparison without considering

how changes in water flux (and thus driving pressure) impact sieving of solutes. Second, external concentration polarization effects are neglected since they rely on system specific considerations such as channel geometry and crossflow velocity. Under these conditions, the observed sieving coefficient, the ratio of the solute concentration in the filtrate to that in the feed solution, will simply be equal to S_∞.

2.2. Partition coefficient

The partition coefficient, which relates the solute concentration just inside the membrane pore to the concentration just outside the pore, approaches unity for completely passed solutes and zero for completely rejected solutes. The partition coefficient can be calculated through

$$\phi_{\text{slit}} = \frac{\langle c_0 \rangle}{c_{b,m}} = \int_0^{1-\lambda-(d_0/h)} g(\rho)d\rho \qquad \text{Eq 5}$$

$$\phi_{\text{cyl}} = \frac{\langle c_0 \rangle}{c_{b,m}} = \int_0^{1-\lambda-(d_0/r_p)} 2\rho g(\rho)d\rho \qquad \text{Eq 6}$$

for slit pores and cylindrical pores, respectively, where $g(\rho)$ is the potential function at some non-dimensional position ρ in the pore and d_o is the Born repulsion limit of approximately 0.187 nm [9][10]. The upper limit in the integration used to evaluate the partition coefficient depends on the ratio of the solute to pore size, $\lambda = r_s/h$ or $\lambda = r_s/r_p$. For the purely steric case, Eq 5 and Eq 6 simplify to $\phi_{slit,steric} = 1 - \lambda$ and $\phi_{cyl,steric} = (1 - \lambda)^2$, respectively, assuming that the Born repulsion term is negligible. Therefore, when the slit pore and cylindrical pore steric partition coefficients are equal, there will necessarily be a difference in pore size for the slit and cylindrical cases given the same solute. The potential function can be represented by a Boltzmann distribution through $g(\rho) = \exp(-E(\rho)/kT)$, where $E(\rho)$ is the energy at a given non-dimensional pore position ρ, k is the Boltzmann constant, and T is temperature [10]. The osmotic reflection coefficient, which was also calculated in our previous work [5], is neglected here for the sake of simplification. This omission is justified due to the much larger impact of the partition coefficient on solute sieving.

2.3. Hindrance factors

Existing correlations can be applied to determine the diffusive and convective hindrance factors for slit pores and circular pores [11]. Most analyses make use of the centerline approximation, with the value of hindrance factor assumed to be constant throughout the pore with the value calculated for the solute at the pore centerline. For slit pores, the hindrance factor can be calculated as [11]

$$K_{c,\text{slit}}=\frac{1}{2}(3-(1-\lambda)^2)\left(1-\frac{\lambda^2}{3}\right)$$

Eq 7

which is valid up to approximately $\lambda = 0.5$. The corresponding circular pore approximation is

$$K_{c,\text{cyl}}=\frac{(2-(1-\lambda)^2)K_s}{2K_t}$$

Eq 8

Where,

$$\begin{pmatrix} K_t \\ K_s \end{pmatrix} = \frac{9}{4}\pi^2 \sqrt{2}(1-\lambda)^{-5/2}\left[1+\sum_{n=1}^{2}\begin{pmatrix} a_n \\ b_n \end{pmatrix}(1-\lambda)^n\right] + \sum_{n=0}^{4}\begin{pmatrix} a_{n+3} \\ b_{n+3} \end{pmatrix}(\lambda)^n.$$

Eq 9

The values for the constants a_n and b_n are shown in Table 1.

2.4. Surface element integration for cylindrical and slit pores

The surface element integration approach has been applied to determine the interaction energy between the solute and membrane surface [5]. This method has been applied previously for cylindrical pores [10][12][13] and has been recently developed for slit pores by our research group [5]. The expression for the energy of a sphere at a given pore position is

$$E_{\text{slit}}(x)=2\pi\int_0^{r_s}\Delta G\left(h-x-r_s\sqrt{1-r^2/r_s^2}\right)\text{rdr}+2\pi\int_0^{r_s}\Delta G\left(h-x+r_s\sqrt{1-r^2/r_s^2}\right)\text{rdr}$$

Eq 10

$$E_{\text{cyl}}(x)=4\int_0^{r_p}\int_0^{\pi}\Delta G\left(-x\cos\theta+\sqrt{r_p^2-x^2\sin^2\theta}-\sqrt{r_s^2-z^2}\right)\sqrt{r_s^2-z^2}d\theta dz$$

Eq 11

where x is the lateral position of the solute center from the pore center, r is the radial distance of a differential surface element from the solute centerline, z is the lateral distance of a differential surface element from the solute center, and θ is the angle of a differential surface area element from some position on the solute surface in a cylindrical pore. The cylindrical and slit pore geometries are depicted in Figure 1. The intermolecular forces are

functions of the distance between the pore surface and solute surface element. Therefore, the interaction energy will also vary with distance as follows

$$\Delta G^{\text{LW}}(L) = -A/12\pi L^2 \quad \text{Eq 12}$$

$$\Delta G^{\text{AB}}(L) = \Delta G^{\text{AB}}_o \exp\left(\frac{d_o - L}{D}\right) \quad \text{Eq 13}$$

$$\Delta G^{\text{EL}}(L) = 2\pi\varepsilon_o\varepsilon_r(\psi_1^2+\psi_2^2)\left(1 - \coth(\kappa L) + \frac{2\psi_1\psi_2}{\psi_1+\psi_2}\operatorname{csch}(\kappa L)\right) \quad \text{Eq 14}$$

for the LW, AB, and EL components, respectively. In Eq 12, Eq 13, and Eq 14, L is the distance between two differential area elements, A is the Hamaker constant for Lifshitz van der Waals interactions, ΔG^{AB}_o is the AB interaction at contact, D is the AB decay length, ε_o is the vacuum permittivity, ε_r is the relative permittivity, ψ_1 and ψ_2 are the surface potentials of the solute and membrane, and κ is the inverse Debye length. The Hamaker constant is itself a function of the LW free energy of interaction at contact such that $A = -12\pi d_o^2\Delta G^{\text{LW}}_o$. The AB (hydration repulsion) force can exhibit oscillatory behavior or it can monotonically decrease with distance depending on surface composition and roughness [14][15].

2.5. Determining LW and AB interaction components

The total interaction energy has contributions associated with the Hamaker constant (LW), the surface potential (EL), and the acid-base free energy of interaction (AB). The van Oss-Good-Chaudhury (VCG) method can be applied in order to isolate the Hamaker constant and the Gibbs free energy for acid-base interaction at contact using goniometric measurements, and values for the surface potential of protein and membrane can be easily determined using literature data for surface charge and zeta potential. Details of this method are discussed in greater detail in other work [9].

2.6. Modeled systems

In this paper, we consider two interacting solute-membrane pairs: 1) beta-2-microglublin (B2M) solute and a polyethylene glycol coated silicon nanopore membrane (PEG-SNM), and 2) bovine serum albumin (BSA) and the same PEG-SNM membrane. These solute-membrane pairs were chosen because they are clinically relevant and have been well characterized in the literature [10]. Interaction energy parameters for both systems are provided in Table 2.

3. Results and Discussion

3.1. XDLVO impact on partition coefficient

The impact of the different XDLVO energy components on the partition coefficients for a solute the size of B2M in slit and cylindrical pores is illustrated in Figure 2. Calculations were performed over a range of pore size, with the solute size fixed at $r_s = 1.59$ nm, with the results plotted as a function of the calculated values of the partition coefficient determined using purely steric interactions. Note that for a given value of the steric partition coefficient, slit pores and cylindrical pores will necessarily exhibit different pure water permeabilities. The output is shown for LW, AB (with $D = 0.11$ nm and $D = 0.6$ nm) and EL interactions. Values for the acid-base decay constant can vary significantly, with $D = 0.11$ nm taken from our previous study [5] and $D = 0.6$ nm appearing elsewhere in the literature [10]. It is clear from the model calculations that XDLVO interactions can both increase (attractive forces) and decrease (repulsive forces) the partition coefficient compared to the purely steric case. Smaller values of the Hamaker constant appear to have an almost negligible effect on the partition coefficient, while $A = 10 \times 10^{-21}$ J corresponds to a notable change from the steric case. This demonstrates that the attractive LW interactions can be significant, although in practice they do not tend to operate in isolation and thus such high partition coefficients are unlikely to be physically realizable. The cylindrical pore exhibits a larger partition coefficient under purely LW conditions than the slit pore. The cases of larger AB interactions ($D = 0.6$ nm) and larger EL solute surface potentials lead to significantly lower partition coefficients than predictions based only on steric interactions. Interestingly, for all three solute surface potentials, there is virtually no difference in the ϕ_{EL} value between cylindrical and slit pores. This suggests that EL interactions, which decay at a slower rate than AB or LW interactions, do not depend significantly on the nanoscale geometry.

3.2. Permeability-selectivity tradeoff

The scaled permeability is plotted as a function of the solute (B2M) selectivity in Figure 3. The data are modeled for the steric case and full XDLVO case (with $D = 0.11$ nm and $D = 0.6$ nm). Calculations were performed over a range of pore size, with the permeability and selectivity calculated for each value of r_p or h. As noted in earlier work, slit pores offer greater selectivity than cylindrical pores at a given value of the scaled permeability [4]. At very large values of the scaled permeability, the selectivities for both cylindrical and slit pores approach a value of one since the very large pores provie minimal exclusion of the solute passage in both pore geometries. When $D = 0.11$ nm, the selectivity curves for both pore types are shifted slightly to the right, corresponding to a higher selectivity at a given permeability since the repulsive XDLVO interactions decrease the solute sieving coefficients (and thus increase the selectivity) for a given permeability [10][5]. Interestingly, for $D = 0.11$ nm, the differences in selectivity between the cylindrical and slit pores are very similar to those for the purely steric case over the entire range of pore size. Calculations using a larger AB decay length ($D = 0.6$ nm), show a significantly greater difference in the selectivity profiles for the two pore geometries, with the slit pore demonstrating much greater selectivity at a given scaled permeability than the cylindrical pore. These results suggest that XDLVO interactions can have a different impact on solute selectivity depending upon the pore geometry.

3.3. BSA-B2M selectivity

In designing membranes for biological applications, pore sizes are engineered to optimize sieving and rejection of different solutes. For example, in kidney hemofiltration it is desirable to remove middle molecular weight solutes such as B2M while retaining large solutes such as BSA. Therefore, the ratio of BSA selectivity to B2M selectivity is an important design parameter. In Figure 4, this ratio has been plotted against the scaled permeability. Slit pores exhibit a much higher BSA to B2M selectivity than cylindrical pores. For a wide range of values, the slit pore ratio is above 10^3 while the cylindrical pore value is significantly lower. Accounting for XDLVO interactions, the BSA-B2M selectivity ratio curves shift to the right so that greater BSA-B2M selectivity is achieved at larger scaled permeabilities. As the scaled permeability increases, and B2M becomes increasingly small relative to the pore size (conditions where the XDLVO effects for B2M also become unimportant), XDLVO interactions for BSA remain significant. Therefore, the effect of the XDLVO interactions on the selectivity ratio becomes greater due to the increase in BSA selectivity. Unsurprisingly, this effect is larger for $D = 0.6$ nm than for $D = 0.11$ nm due to greater XDLVO repulsion between solute and membrane at the larger decay constant value. The slit pore membrane retains a very high selectivity ratio ($>10^3$) even at scaled permeability values of 10×10^{-18} m^2 (when including XDLVO interactions), while the cylindrical pore membrane has a selectivity of less than 5 under identical conditions.

4. Conclusion

The aim of this study was to compare, from a theoretical standpoint, the selectivity of slit and cylindrical pore membranes while accounting for both steric and XDLVO interactions. Although both the cylindrical pore and slit pore models have already seen some form of experimental validation in earlier studies [5][10], the performance of these membranes for protein separations, with a focus on hemofiltration, has not previously been examined. As MEMS technology becomes increasingly mature, it should be possible to create cylindrical pore SNM using nanolithography techniques [16] comparable to those used previously to produce slit pore membranes. Thus, future studies could experimentally validate the results of this study using membranes of the same material and nanoscale thickness as our SNM.

In this study, the impact of the AB and EL contributions to the XDLVO partition coefficient for B2M were considered. For all cases, the slit pore XDLVO partition coefficient was lower than the cylindrical value, suggesting that these interactions disproportionately hinder transport through slit pore membranes. Interestingly, for EL interactions there is virtually no difference between the partition coefficient values in the slit and cylindrical pores. Evaluating the B2M selectivity as a function of the scaled hydraulic permeability demonstrates that incorporating XDLVO interactions magnifies the existing disparities between the selectivity in slit and cylindrical pores. In particular, at larger values of the AB decay constant, the slit pore selectivity is significantly greater than the selectivity in a membrane with cylindrical pores. Finally, the BSA to B2M selectivity ratio is much greater in membranes with slit pores than cylindrical pores, indicating that slit pore membranes would be particularly well suited for applications such as hemofiltration that require highly selective transport.

The results of this study have significant implications for the application of SNM in membrane processes where high selectivity of biomolecules is desirable. Although many factors are important in selecting a membrane for a given application, the results presented in this study clearly demonstrate that when membrane thickness and material are held constant, optimizing for a slit pore geometry leads to a more favorable selectivity ratio in hemofiltration compared to that for a cylindrical pore geometry. This provides further support for ongoing efforts to develop high performance slit pore membranes for use in hemofiltration and in implantable renal assist devices.

Acknowledgments

References

1. Fissell WH, Dubnisheva A, Eldridge AN, Fleischman AJ, Zydney AL, Roy S. High-performance silicon nanopore hemofiltration membranes. J Memb Sci. 2009; 326:58–63. DOI: 10.1016/j.memsci.2008.09.039 [PubMed: 20054402]

2. Fissell WH, Roy S, Davenport A. Achieving more frequent and longer dialysis for the majority: wearable dialysis and implantable artificial kidney devices. Kidney Int. 2013; 84:256–64. DOI: 10.1038/ki.2012.466 [PubMed: 23407434]

3. Smith RA, Goldman K, Fissell WH, Fleischman AJ, Zorman Ca, Roy S. Removal of endotoxin from deionized water using micromachined silicon nanopore membranes. J Micromechanics Microengineering. 2011; 21:54029.doi: 10.1088/0960-1317/21/5/054029

4. Kanani DM, Fissell WH, Roy S, Dubnisheva A, Fleischman A, Zydney AL. Permeability-Selectivity Analysis for Ultrafiltration: Effect of Pore Geometry. J Memb Sci. 2010; 349:405.doi: 10.1016/j.memsci.2009.12.003 [PubMed: 20161691]

5. Feinberg BJ, Hsiao JC, Park J, Zydney AL, Fissell WH, Roy S. Silicon nanoporous membranes as a rigorous platform for validation of biomolecular transport models. J Memb Sci. 2017

6. Wang J, Dlamini DS, Mishra AK, Pendergast MTM, Wong MCY, Mamba BB, Freger V, Verliefde ARD, Hoek EMV. A critical review of transport through osmotic membranes. J Memb Sci. 2014; 454:516–537. DOI: 10.1016/j.memsci.2013.12.034

7. Deen, WM. Analysis of transport phenomena. Oxford University Press; New York: 1998.

8. Opong W, Zydney A. Diffusive and convective protein transport through asymmetric membranes. AIChE J. 1991; 37:1497–1510. [accessed September 12, 2014] http://onlinelibrary.wiley.com/doi/10.1002/aic.690371007/abstract.

9. Van Oss, CJ. Interfacial forces in aqueous media. CRC press; 2006.

10. Bhattacharjee S, Sharma A, Bhattacharya P. Estimation and influence of long range solute. Membrane interactions in ultrafiltration. Ind Eng Chem Res. 1996; 35:3108–3121. http://pubs.acs.org/doi/abs/10.1021/ie9507843.

11. Dechadilok P, Deen WM. Hindrance factors for diffusion and convection in pores. Ind Eng Chem Res. 2006; 45:6953–6959. DOI: 10.1021/ie051387n

12. Bhattacharjee S, Elimelech M. Surface element integration: a novel technique for evaluation of DLVO interaction between a particle and a flat plate. J Colloid Interface Sci. 1997; 193:273–285. doi:10.1006/jcis. 1997.5076. [PubMed: 9344528]

13. Bhattacharjee S, Chen JY, Elimelech M. DLVO interaction energy between spheroidal particles and a flat surface, Colloids Surfaces A Physicochem. Eng Asp. 2000; 165:143–156. DOI: 10.1016/S0927-7757(99)00448-3

14. Donaldson SH, Valtiner M, Gebbie Ma, Harada J, Israelachvili JN. Interactions and visualization of bio-mimetic membrane detachment at smooth and nano-rough gold electrode surfaces. Soft Matter. 2013; 9:5231–5238. DOI: 10.1039/c3sm27217f

15. Israelachvili, JN. Intermolecular and surface forces: revised third edition. Academic press; 2011.

16. Storm AJ, Chen JH, Ling XS, Zandbergen HW, Dekker C. Fabrication of solid-state nanopores with single-nanometre precision. Nat Mater. 2003; 2:537–540. [PubMed: 12858166]
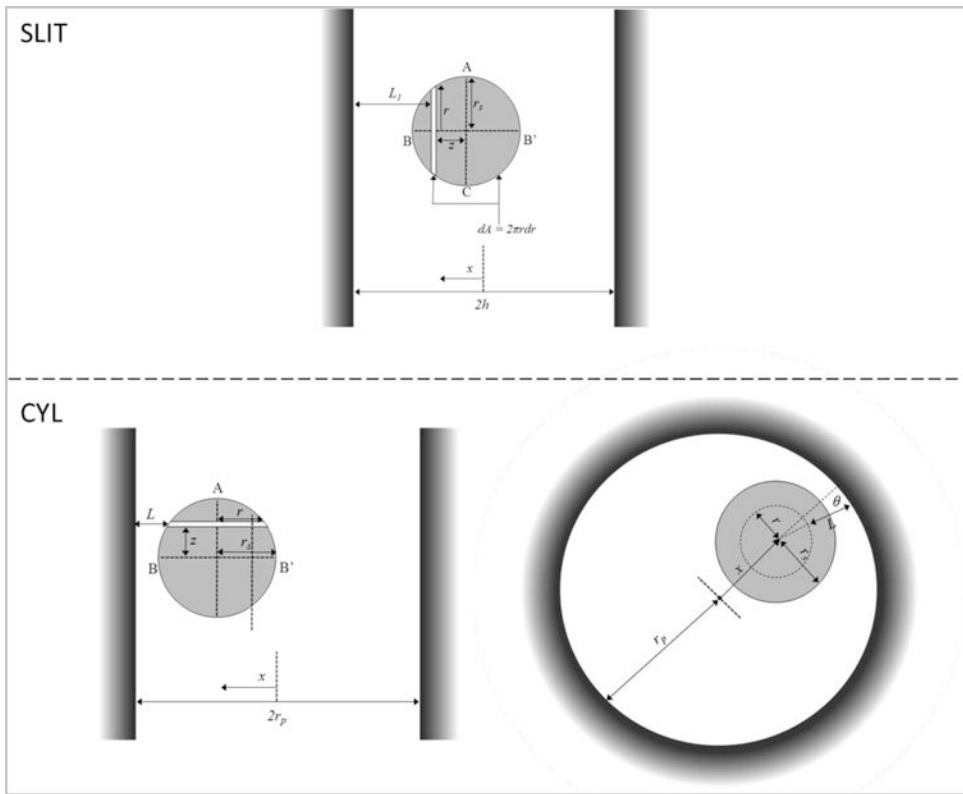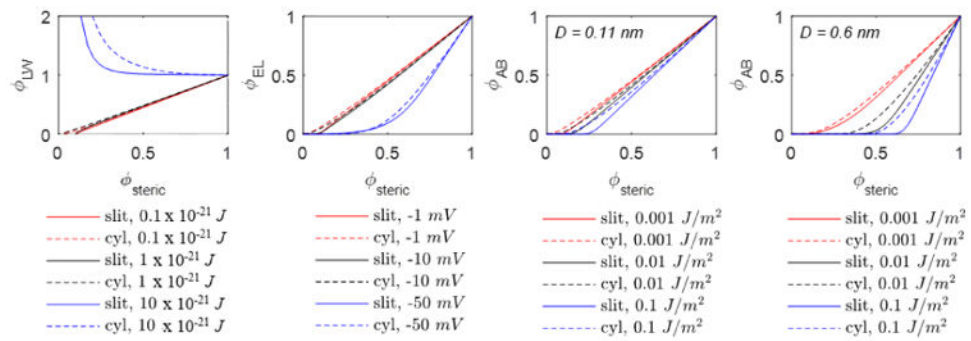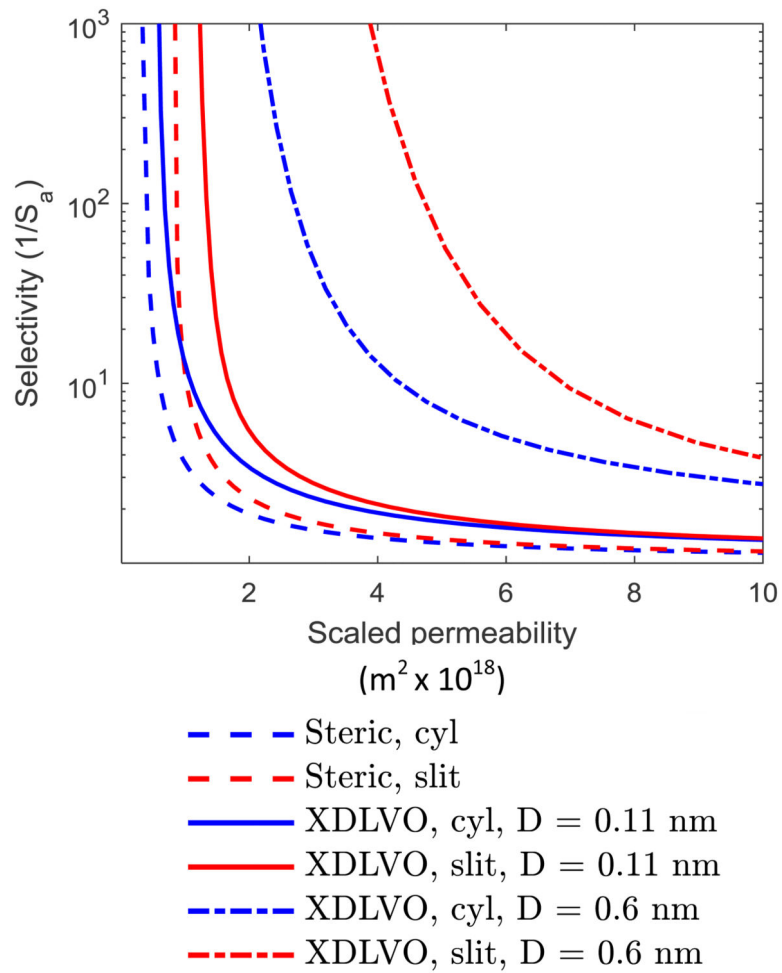
Figure 1.
Cross section graphical representation of solute positioned in slit pore (SLIT) and cylindrical pore (CYL).
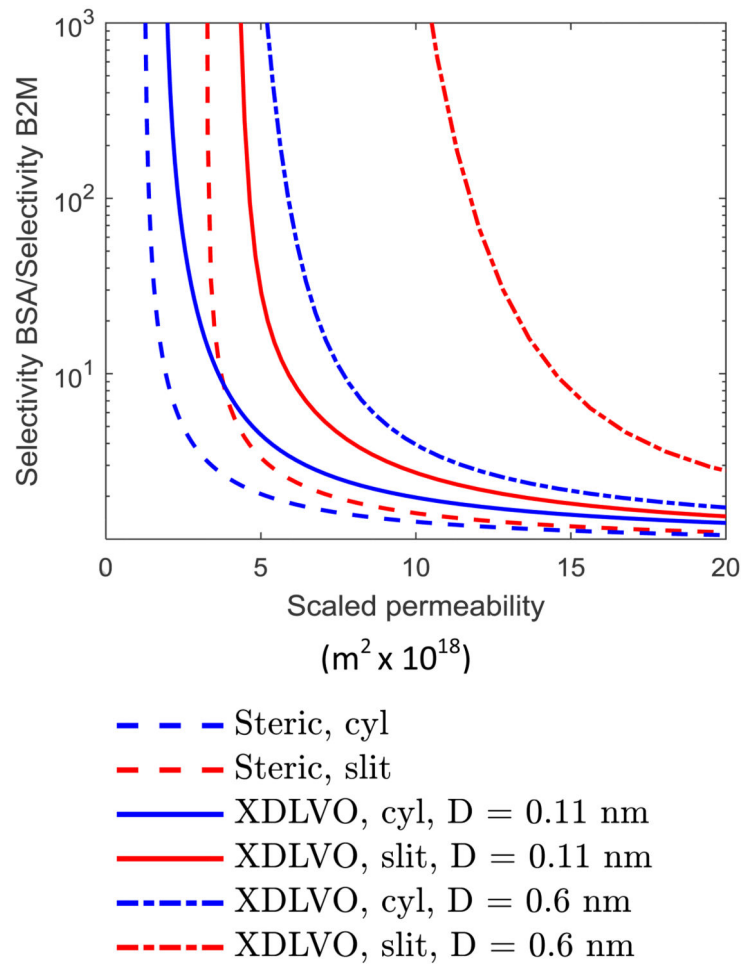
Figure 2.
The partition coefficient with LW interactions, AB interactions (with an AB decay length of 0.11 and 0.6 nm) or EL interactions as a function of the steric partition coefficient. Results are shown for different values of the LW Hamaker constant, AB interaction at contact, and EL solute surface potential.

Figure 3.
The chang in B2M selectivity with scaled hydraulic permeability for cylindrical and slit pores with and without XDLVO interactions.

Figure 4.
The dependence of the B2M to BSA selectivity ratio on the scaled hydraulic permeability for cylindrical and slit pores with and without XDLVO interactions.

Table 1

Constant values for determining the cylindrical pore hindrance factors [10].

n	a_n	b_n
1	-73/60	7/60
2	77293/50400	-2227/50400
3	-22.5083	4.018
4	-5.6117	-3.9788
5	-0.3363	-1.9215
6	-1.216	4.392
7	1.647	5.006

Table 2

Interaction energy constants and feed solution parameters for Systems 1 and 2 [5][10].

Interaction energy constants	System 1	System 2	
Solute	B2M	BSA	
Surface	PEG-SNM	PEG-SNM	
Hamaker Constant (A)	4.61×10^{-21}	1.99×10^{-21}	J
G_o^{AB}	41	54	mJ/m^2
Surface potential (Solute)	-4	-20	mV
Surface potential (Surface)	-12	-12	mV
Feed solution parameters			
pH	7.2		
Ionic strength	0.14		M